Earth and Planetary Science Letters 549 (2020) 116495

Contents lists available at ScienceDirect

Earth and Planetary Science Letters

www.elsevier.com/locate/epsl

Magnetite biomineralization in ferruginous waters and early Earth evolution

K.W. Bauer [a,1], J.M. Byrne [b], P. Kenward [a], R.L. Simister [a], C.C. Michiels [a], A. Friese [c], A. Vuillemin [c,2], C. Henny [d], S. Nomosatryo [c,d], J. Kallmeyer [c], A. Kappler [b], M.A. Smit [a], R. Francois [a], S.A. Crowe [a,*]

[a] Department of Microbiology and Immunology and Department of Earth, Ocean and Atmospheric Sciences, The University of British Columbia, 2020 - 2207 Main Mall, Vancouver, British Columbia V6T 1Z4, Canada
[b] Center for Applied Geosciences, University of Tuebingen, 72076 Tuebingen, Germany
[c] GFZ German Research Centre for Geosciences, Helmholtz Centre Potsdam, 14473 Potsdam, Germany
[d] Research Center for Limnology, Indonesia Institute of Sciences (LIPI), Cibinong Science Centre, Cibinon-Bogor, Indonesia

ARTICLE INFO

Article history:
Received 9 January 2020
Received in revised form 16 July 2020
Accepted 20 July 2020
Available online xxxx
Editor: F. Moynier

Keywords:
Earth evolution
geochemistry
banded iron formations
magnetite
ferruginous oceans

ABSTRACT

Burial of large quantities of magnetite ($Fe(II)Fe(III)_2O_4$) in iron formations (IFs) likely contributed to the protracted oxidation of Earth's surface during the Precambrian Eons. Magnetite can form through a diversity of biological and abiotic pathways and its preservation in IFs may thus be variably interpreted as the result of some combination of these processes. Such interpretations give rise to divergent pictures of the Precambrian Earth system and models for its evolution through time. New knowledge on the contribution of specific magnetite formation pathways is, therefore, needed to accurately tether our conceptual and numerical models to the geologic record. To constrain pathways of magnetite formation under ferruginous conditions, we conducted geochemical and multi-method microspectroscopic analyses on particles obtained from the water columns and sediments of ferruginous lakes Matano and Towuti, in Indonesia. We find that biologically reactive Fe(III) mineral phases are reduced in the anoxic waters of both lakes, causing the formation of primary authigenic magnetite, directly in the water column. This water column magnetite often takes conspicuous framboidal forms, which given the link to microbial Fe(III) reduction, may provide a biological signature on early Earth and by extension, other planetary bodies. The consumption of more biologically reactive forms of Fe(III) and the resulting delivery of primary magnetite to underlying sediments promotes the burial of oxidized equivalents and implies that primary magnetite formation could have been a principal pathway of Fe delivery to IFs. Combined, the removal of Fe from Earth's surface through biologically induced magnetite formation and subsequent burial in IFs, suggests that seawater chemistry and the microbially mediated reactions that cause magnetite formation played key roles in Earth system evolution and in setting the pace for planetary oxidation through the Precambrian Eons.

1. Introduction

Biogeochemical cycling of iron (Fe) and carbon (C) plays a key role in setting Earth's surface redox budgets and climate. Burial of reduced forms of C and Fe in marine sediments as organic matter (OM) and ferrous Fe (Fe(II))-bearing minerals, in particular, oxidize Earth's surface and represent quantitatively important net sources of oxygen to the modern atmosphere (Catling and Claire, 2005; Holland, 2006). Oxidation of crust-derived Fe(II) to form Fe(III)-bearing minerals, by contrast, is a net sink for atmospheric oxygen (Holland, 2002). The magnitudes of these sources and sinks are influenced by dynamics in coupled C and Fe cycling, which can induce secular variation in Earth's surface chemistry (Catling and Claire, 2005; Holland, 2002, 2006; Kasting, 2013) and, over geological timescales, lead to fundamentally different ocean-atmosphere redox states and climate systems (Holland, 2002; Kasting, 2013).

During much of the Precambrian Eons, the ocean-atmosphere system was nearly oxygen-free and rich in reduced chemical species (Fe(II), H_2 and CH_4) (Zerkle et al., 2012). Widespread

* Corresponding author.
E-mail address: sean.crowe@ubc.ca (S.A. Crowe).
[1] Current address: Department of Earth Sciences, University of Hong Kong, Pokfulam Road, Hong Kong SAR.
[2] Current address: Department of Earth and Environmental Sciences, Paleontology and Geobiology, Ludwig-Maximilians-Universität, Richard-Wagner-Str. 10, 80333 Munich, Germany.

https://doi.org/10.1016/j.epsl.2020.116495
0012-821X/

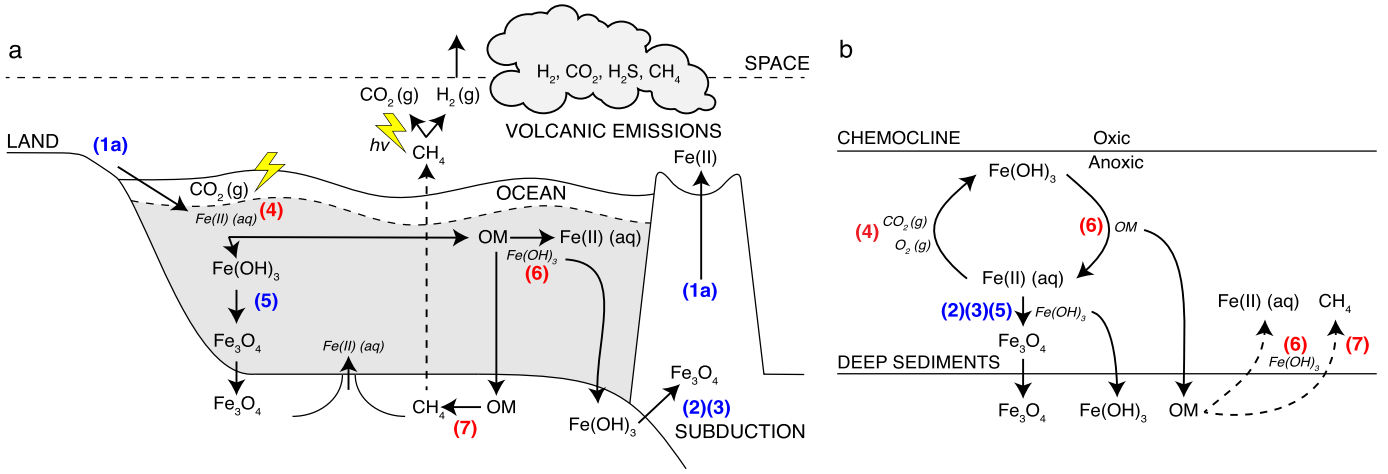

Fig. 1. Schematic diagram showing the influence of magnetite formation on redox budgets. The numbers correspond to the different reactions presented in the introduction. Blue colored reactions are abiotic, whereas red colored reactions are microbially controlled. **a)** Schematic diagram illustrating the principle reactions controlling the redox state of Fe in the ocean-atmosphere system. **b)** A schematic diagram displaying a detailed view of Fe and C cycling under ferruginous water column conditions. (For interpretation of the colors in the figure(s), the reader is referred to the web version of this article.)

deposition of Fe minerals at this time formed sedimentary iron formations (IFs) as the result of coupled C and Fe cycling in the oceans. Today, these deposits contain vast quantities of both ferric [Fe(III)] and ferrous [Fe(II)] iron, the ratio of which can vary appreciably across IF facies leading to an overall mean iron redox state of 2.6 (Klein, 2005). IF mineralogy, notably, is dominated by the mixed-valence oxide magnetite ($Fe^{2+}Fe^{3+}_2O_4$) (Klein, 2005), and burial of magnetite in IFs played an important role as a sink for Fe and in setting the redox state of IFs with implications for evolution of the ocean-atmosphere system (Holland, 2002; Johnson et al., 2008). The oxidation of crustal Fe(II) to form Fe(III) buried as magnetite in IFs represented a net oxidant sink for the Earth's surface, which would have ultimately led to the production of H_2 as the corresponding sink for reduced equivalents (reaction 1);

$$3FeO + H_2O \rightarrow Fe_3O_4 + H_2 \quad (1)$$

Such H_2 production promotes planetary oxidation when H_2 is lost to space (Holland, 2002; Kasting, 2013). The net effect of magnetite burial in IFs on Earth's global redox budget is represented by reaction (1) and is the same regardless of the pathway through which it forms. The factors controlling magnetite formation and burial in IFs and the ultimate production of hydrogen, however, such as coupled C and Fe cycling directly in the oceans or diagenetic and metamorphic reactions, can be very different (Fig. 1). This has important implications for interpretations of Precambrian seawater chemistry and biology.

The precise pathways for magnetite formation and ultimate burial in IFs remain poorly constrained and thus models that aim to mechanistically link the deposition of IFs to the evolution of Earth's surface redox budgets remain uncertain. Magnetite formation in IFs is widely attributed to diagenetic and or metamorphic reactions (Johnson et al., 2008; Konhauser et al., 2005). Magnetites contained in IFs exhibit low-grade metamorphic textures, implying recrystallization of primary IF mineral assemblages and the overprinting of original fabrics (Klein, 2005; Li et al., 2013; Lovley, 1991). Many diagenetic and metamorphic models for magnetite formation suggest primary Fe deposition as Fe(III) (oxyhydr)oxides (ferrihydrite, goethite) (Klein, 2005) and mixed valence (oxyhydr)oxides (green rust) (Halevy et al., 2017; Zegeye et al., 2012), which may then react with Fe(II) (reaction 1a, Fig. 1a) in later-stage diagenetic (reaction 2) and thermochemical (reaction 3) reactions, transforming these precursor phases to magnetite;

$$FeO + 2H^+ \rightarrow Fe^{2+} + H_2O \quad (1a)$$

$$Fe^{2+} + 2Fe(OH)_3 + 2OH^- \rightarrow Fe_3O_4 + 4H_2O \quad (2)$$

$$Fe_2O_3 + Fe^{2+} + H_2O \rightarrow Fe_3O_4 + 2H^+ \quad (3)$$

Notably, magnetite formation via reactions (2) and (3) is not necessarily the direct product of coupled C and Fe cycling in the oceans. Thus magnetite formed in this way is decoupled from the physicochemical and biological conditions and processes in the ocean-atmosphere system at the time of IF deposition. In contrast, precipitation and burial of primary magnetite in IFs would directly link IF mineralogy to the principal water column processes that cause IF deposition.

Precipitation of primary magnetite directly in the water column of the Precambrian oceans may also have been possible, as magnetite forms in laboratory experiments as the product of biological processes including magnetosome formation in magnetotactic bacteria (Blakemore, 1975), anoxygenic Fe(II) photosynthesis (Jiao et al., 2005) and Fe(III) respiration (Lovley, 1991). These processes were all likely widespread under ferruginous ocean conditions (Halevy et al., 2017; Konhauser et al., 2005; Tosca et al., 2016). Magnetite formation through these latter processes occurs by abiotic reaction of seawater Fe(II) with Fe(III) (oxyhydr)oxides produced either through reaction with oxygen generated through oxygenic photosynthesis, or directly through microbial anoxygenic photosynthesis with Fe(II) as the electron donor (reactions 4 and 5);

$$4Fe^{2+} + HCO_3^- + 10H_2O \rightarrow CH_2O + 4Fe(OH)_3 + 7H^+ \quad (4)$$

$$Fe^{2+} + 2Fe(OH)_3 + 2OH^- \rightarrow Fe_3O_4 + 4H_2O \quad (5)$$

The extent to which such processes lead to magnetite formation depends on the concentration of Fe(II) in seawater, production rate of Fe(III) (oxyhydr)oxides, and other physicochemical parameters such as pH, temperature and settling velocity. The organic C produced via anoxygenic photosynthesis (reaction 4), furthermore, may also be consumed in microbial metabolisms like anaerobic Fe(III) respiration (reaction 6) and fermentation (reaction 7), reactions that can fuel competing Fe mineralization pathways;

$$CH_2O + 4Fe(OH)_3 + 7H^+ \rightarrow 4Fe^{2+} + HCO_3^- + 10H_2O \quad (6)$$

$$CH_2O + H_2O \rightarrow 2H_2 + CO_2 \quad (7)$$

Organic C not consumed by Fe(III) reduction may be channeled through fermentation (reaction 7), producing H_2 and dissolved inorganic carbon species (DIC). High concentrations of DIC and Fe(II) in turn tend to favor the formation of the reduced Fe-carbonate mineral siderite over magnetite (Zachara et al., 1998). The organic C consumed via reaction (7), furthermore, is not buried and also produces an equivalent 2 mol of H_2, promoting H_2 loss to space (Kasting, 2013).

The net effect on Earth's redox budget is the same regardless of the locus of magnetite formation (reaction 1), but in contrast to thermochemical and diagenetic pathways (reactions 2 and 3), water column magnetite formation would be directly controlled by and thus record primary information on the chemistry and ecology of ancient seawater. Importantly, the formation of water column magnetite (reactions 4 and 5) would tend to inhibit microbial Fe(III) reduction (reaction 6), as Fe(III) sequestered in magnetite is poorly biologically reactive (Kostka and Nealson, 1995) (Fig. 1). At the same time water column magnetite formation would tend to channel organic C from respiration to hydrogen production through fermentation (reaction 7) (Fig. 1). It would thus also implicate the processes responsible for magnetite formation in controlling the deposition of IFs, their mineralogy, oxidation state, and corresponding influences on Earth surface redox budgets. While low temperature magnetite precipitation in modern soils and sediments is frequently observed (Karlin et al., 1987), primary water column magnetite formation and its role in IF deposition and early Earth evolution is seldom considered.

Modern ferruginous environments provide natural laboratories to examine processes extensible to the Fe-rich Precambrian oceans (Crowe et al., 2008; Lambrecht et al., 2018; Vuillemin et al., 2019a, 2019b; Walter et al., 2014). To investigate Fe-cycling and mineral formation under ferruginous conditions we conducted experiments in, and collected samples from Lakes Matano and Towuti (herein referred to as LM and LT) on Sulawesi Island, Indonesia. LM and LT are part of the interconnected Malili Lakes system. The catchment basin surrounding the lakes is dominated by ultramafic rocks of ophiolitic origins and weathering of these rocks led to development of exceptionally Fe-rich lateritic soils (Crowe et al., 2008). Heavy tropical rains deliver strong fluxes of Fe (oxyhydr)oxides from these soils to the lakes, which exert an overwhelming influence on the lakes' biogeochemistry (Crowe et al., 2008). Both LM and LT are physically and chemically stratified and characterized by persistently anoxic, Fe(II)-rich ($\sim$140 and $\sim$10 µM respectively), and virtually sulfate free ($<$5 µM) deep waters (Crowe et al., 2014b) (Fig. 2). We combined geochemical and mineralogical analyses to evaluate Fe cycling and pelagic Fe mineral formation in both LM and LT, revealing that water column Fe(III) reduction leads directly to the formation of primary authigenic magnetite.

2. Materials and methods

2.1. Sample collection

Sediment trap sampling was performed in May and June 2015. Sediment traps consisting of four tubes (8 cm diameter, 57 cm tall) were deployed at specified depths in each lake (Fig. 2). Traps were deployed for 6.2 and 3.0 days in LM and LT, respectively. During recovery, material from half of the sediment traps (2 of 4 tubes) was immediately filtered onto glass-fiber filters (0.2 µm) using a peristaltic pump, with no exposure to the atmosphere. Filters were transferred directly to 15 ml falcon tubes containing 5 ml 0.5 N HCl. The other half was quantitatively transferred, again avoiding exposure to the atmosphere, into 12 ml Exetainers with no headspace.

Sediment and water samples were recovered from both lakes in years 2014 and 2015. Water temperature, oxygen concentration, light intensity, and transmissometry were determined in situ with a conductivity-temperature-depth probe (CTD; Sea-Bird, SBE-19; Sea-Bird Electronics, Bellevue, WA, USA). Water samples were collected with 5 L (Niskin; General Oceanics, Miami, FL, USA) bottles attached in series to a stainless-steel cable. The bottles were placed at depth to an accuracy of $\pm$1 m using a commercial fish finder (Furuno, FCV 585; Furuno Electric Co., Nishinomiya, Japan). Sediment cores ($<$0.5 m) were retrieved from both lakes using a gravity corer. Water column pH was determined by inserting the pH electrode (ThermoScientific, Orion) into a glass bottle free of air bubbles containing the water sample. Sediments were recovered at water depths of 200 m in both lakes, which were overlain by anoxic and Fe(II)-rich water. Cores were sectioned in a N_2 flushed glove bag at a resolution of 0.5, 1, and 2 cm resolution for the upper 1, 1-10, and below 10 cm, respectively. A sub-sample of 0.5 g of sediment from each interval was immediately extracted in 1 ml 1 N HCl so that both Fe(II) and Fe(III) could be determined in this reactive (oxyhydr)oxide fraction (Lovley and Phillips, 1986b; Thamdrup et al., 1994), and Fe-speciation on these easily extractable phases was measured on site spectrophotometrically using the ferrozine assay (Viollier et al., 2000). The residual sediment from each section was preserved in falcon tubes and sealed in N_2 flushed aluminum foil bags.

2.2. Magnetite extraction for spectroscopic and geochemical analyses

We prepared magnetic separates from sediments for multi-method spectroscopic analyses and to test the selectivity of the oxalate extraction. To accomplish this, we treated a sub-set of sediments with dithionite, to remove reducible Fe (oxyhydr)oxide mineral phases (Poulton and Canfield, 2005). We then carefully, and as quantitatively as possible, separated magnetic grains from the residual sediment by hand using neodymium magnets. Subsamples of both the magnetic extracts and residual magnetite-free sediment were stored under N_2 for spectroscopic and geochemical analyses.

2.3. Fe-speciation analysis

Sediment Fe-speciation measurements were performed on anoxically preserved and freeze-dried sediment samples following the method of Poulton and Canfield (2005). 100-200 mg of dry sediment was weighed into 15 ml centrifuge tubes, and the extraction scheme was followed as in Poulton and Canfield (2005), only substituting 0.5 M HCl in place of the hydroxylamine hydrochloride leach (Table 1), again, so that both Fe(II) and Fe(III) could be determined in this reactive (oxyhydr)oxide fraction. The highly reactive, "Fe_{HR}" pool is defined as the sum of carbonate-associated Fe ($Fe_{Aca,}$ acetate), (oxyhydr)oxides including ferrihydrite and lepidocrocite ($Fe_{HCl,}$ 0.5 N HCl extractable Fe), ferric (oxyhydr)oxides including hematite and goethite ($Fe_{Dith,}$ dithionite extractable Fe), and magnetite ($Fe_{Oxa,}$ oxalate extractable Fe). The non-reactive, "Fe_{NR}" pool is attributed to Fe in silicate minerals ($Fe_{Sil,}$ near boiling 6 N HCl extractable Fe after removal of reactive phases). Fe-speciation was also conducted on sediment trap material by applying each extraction directly to filters within the 15 ml centrifuge tube. Fe concentration measurements were performed using a Flame Atomic Absorption Spectrophotometer (Flame AAS). Precision on triplicate measurements was $<$1% (2SD) and our limit of detection was $\sim$0.1 µg g^{-1}. Our extractions dissolved $>$92% of the Fe from the PACS-2 international reference standard.

The oxalate leach is known to dissolve non-magnetite phases in some environments (Slotznick et al., 2018) and so we explored oxalate selectivity in LM and LT. The oxalate extraction is highly selective for Fe_{Oxa} (i.e., magnetite) in sediment trap material and deposited sediments from LM and LT, and this gives us confidence

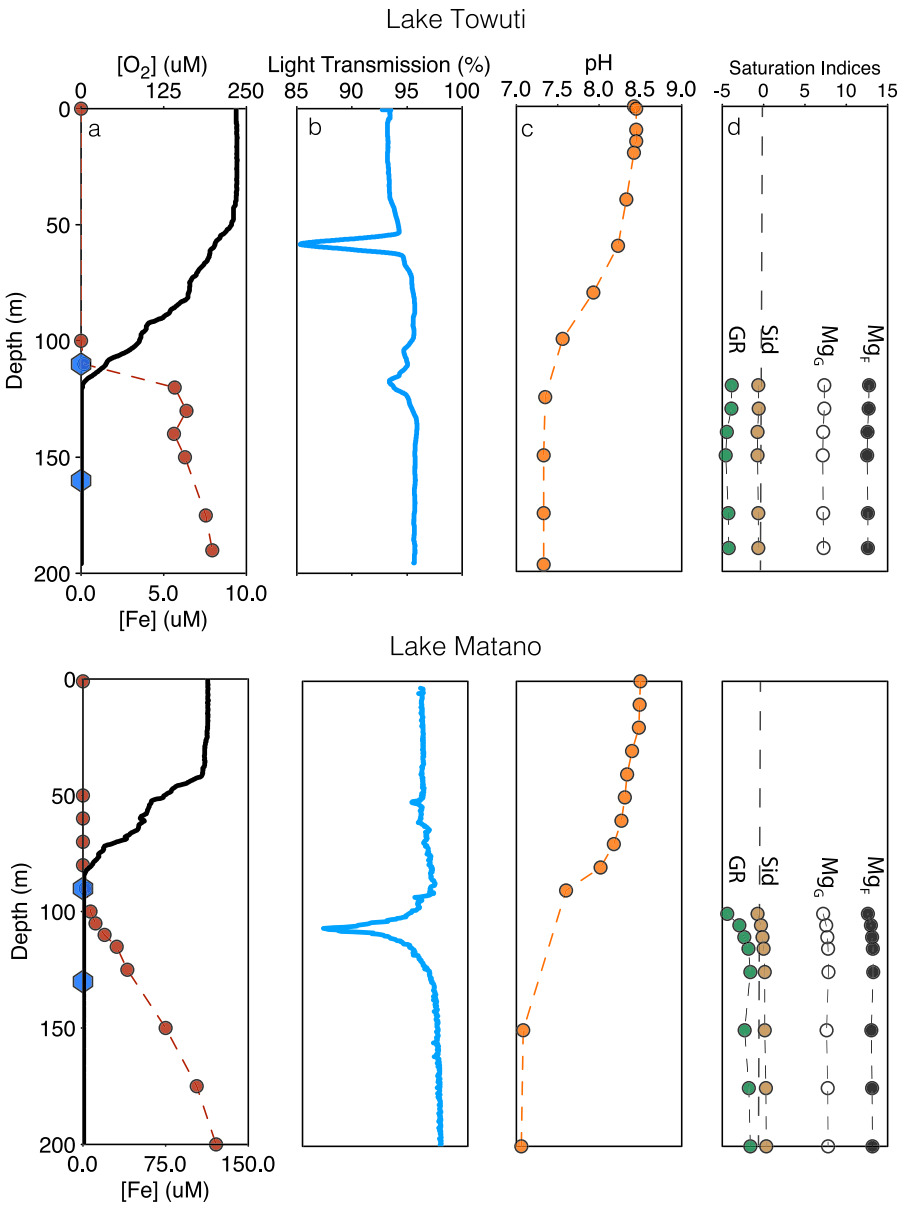

Fig. 2. Chemical and physical properties of LT (top panels) and LM (bottom panels). The blue hexagons on the y-axes represent the sediment trap deployment depths in LT and LM, 110 and 160 m and 90 and 130 m respectively. **a)** Dissolved O_2 and Fe(II). **b)** Light transmission. **c)** pH. **d)** Mineral saturation indices. Closed black circles represent the SI for magnetite calculated using Fe(III) concentrations assuming ferrihydrite saturation (Mg_F). Open black circles represent the SI for magnetite calculated using Fe(III) concentrations assuming goethite saturation (Mg_G). We note both lakes' deep waters are oversaturated with respect to magnetite. Closed brown circles represent the SI for siderite (Sid). Closed green circles represent the SI for carbonate green rust (GR). See Table 2 for minerals reactions and solubility products.

Table 1
Description of Fe speciation extractions. Reactive Fe (Fe_{HR}) refers to the sum of Fe_{Aca}, $Fe(II)_{HCl}$, $Fe(III)_{HCl}$, Fe_{Dith}, and Fe_{Oxa} pools. Unreactive Fe (Fe_{NR}, main text) refers to the Fe_{Sil} pool.

Operationally defined Fe – mineral phases	Extractant
Siderite, Fe_{Aca}	1 M Na-acetate pH 4.5, 24 h (Poulton and Canfield, 2005)
Lepidocrocite, Ferrihydrite, Fe(II) and $Fe(III)_{HCl}$	0.5 M HCl, 1 h (Thamdrup et al., 1994)
Goethite, Hematite, Fe_{Dith}	0.35 M acetic acid/0.2 M Na-citrate Na-dithionite, 2 h (Poulton and Canfield, 2005)
Magnetite, Fe_{Oxa}	0.2 M ammonium oxalate/0.17 M oxalic acid, 6 h (Poulton and Canfield, 2005)
Silicate Fe, Fe_{Sil}	Near boiling 6 M HCl, 24 h (Poulton and Canfield, 2005)

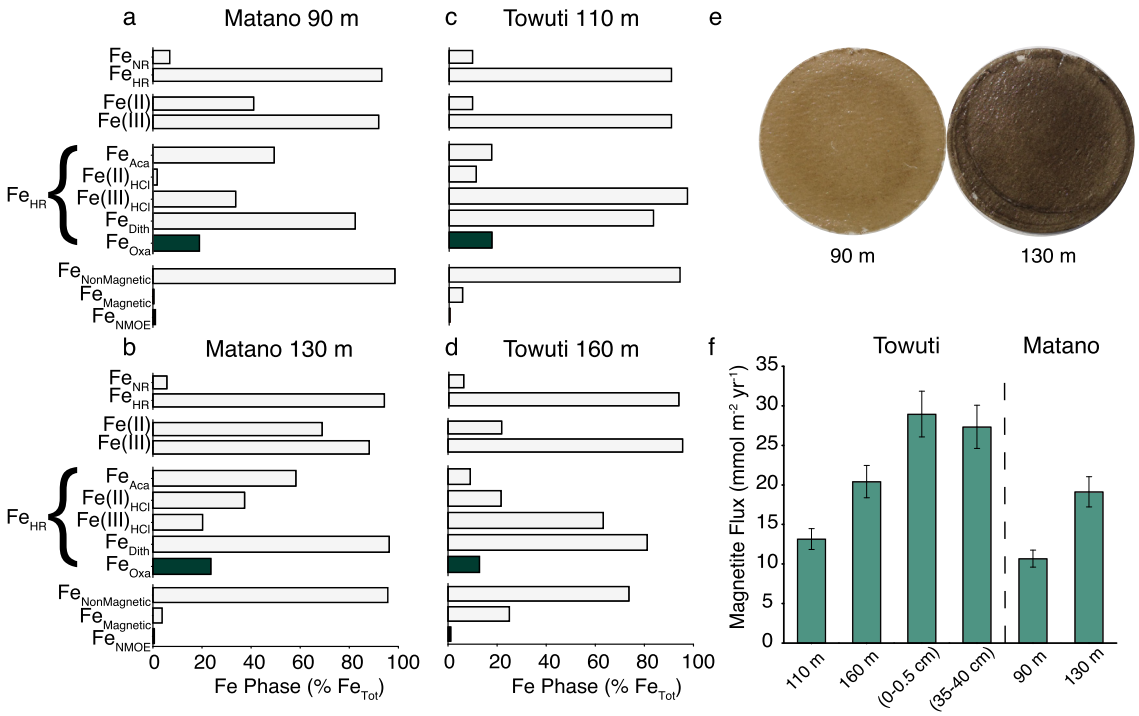

Fig. 3. Malili lake Fe-speciation and magnetite fluxes. **a-d)** Water column Fe-speciation plots. Each operationally defined Fe-phase is normalized to the total Fe content of the sample. $Fe_{Magnetic}$, $Fe_{Non\ Magnetic}$ and Fe_{NMOE} refer to our sediment mass balance oxalate leaching tests. **e)** Photographs of filtered sediment trap material from LM. We note the striking color difference of material sedimenting above (shallow sediment trap, 90 m) and below (deep sediment trap, 130 m) the chemocline. **f)** Magnetite fluxes in the sediment traps and sediments in LM and LT. LT core top samples come from the 0–0.5 cm sediment depth interval, whereas core bottom samples from the 35–40 cm sediment depth interval.

in our ability to identify and quantify Fe_{Oxa} (herein referred to as magnetite) in both sedimenting particulate matter from the water column and deposited sediments. Geochemical and multi-method spectroscopic analyses confirmed that magnetically separated grains (see section 3.2 below) are magnetite ($Fe_{Magnetic}$, Fig. 3, Fig. 4). After physical separation of magnetite grains using a magnet, we also leached the residual non-magnetic material ($Fe_{Non\ Magnetic}$, Fig. 3) with oxalate, recovering <0.1% (<0.8% from deposited sediments) of the total Fe (Fe_{NMOE}, Fig. 3), or less than 1% of the total oxalate extractable Fe. This demonstrates that more than 99% of the Fe extracted with oxalate comes from magnetite and less than 1% from the non-selective extraction of other phases. We thus conclude that, while operationally defined, the oxalate extraction applied here is highly selective for magnetite and yields precise and quantitative information on its abundance in sediment trap material and deposited sediments.

2.4. Fe flux calculations

To calculate water column Fe fluxes, area specific Fe sedimentation rates were determined by dividing the amount of Fe captured by the sediment trap in each operationally defined mineral phase (mmol), by the area of the sediment trap (0.005 m^2) and the deployment time to yield Fe fluxes in units of mmol m^{-2} yr^{-1}. In the deposited sediments, area specific Fe accumulation rates were determined by multiplying volume specific Fe concentrations (mmol m^{-3}) by previously determined sedimentation rates (0.0008 and 0.00019 m yr^{-1} in LM and LT, respectively, Crowe et al. (2008); Russell et al. (2016)) to yield sediment Fe accumulation rates in mmol m^{-2} yr^{-1}. Deep-water diffusive Fe(II) gradients in each lake were determined by multiplying Fe(II) concentration gradients by diffusivity coefficients. Bottom water concentrations of Fe(II) in LM and LT are 0.140 and 0.010 mmol l^{-1}, respectively (Fig. 2), and these dissolved pools are quantitatively oxidized at the chemocline (Fig. 2), driving upward diffusive fluxes of Fe(II). We calculate Fe(II) gradients as 1.5 and 0.6 mM m^{-4} in LM and LT, respectively (Fig. 2). Upward diffusional Fe(II) fluxes were estimated by multiplying the Fe(II) gradients by the eddy diffusivity coefficient (0.1 and 0.6 m^2 d^{-1} in LM and LT respectively (Crowe et al., 2014a; Katsev et al., 2010)). We note that in LM, we were unable to calculate sediment magnetite fluxes, as the lake's steep bathymetry effectively focuses detrital Fe (Fe_{Sil}, see Table 1) to the deeper sediments, diluting authigenic Fe mineral phases.

2.5. Saturation state calculations

Saturation indices were calculated as:

$$SI = -log\frac{IAP}{K_{sp}} \tag{5}$$

where IAP is the ion activity product for the relevant mineral phase and K_{sp} is its corresponding solubility product. Saturation indices greater than 0 indicate that water is supersaturated with respect to the relevant mineral, whereas those less than 0 indicate that water is undersaturated with respect to a given mineral phase (Fig. 2d). Solubility products for all mineral phases were taken from the PHREEQC database (Parkhurst and Appelo, 1999). Mineral precipitation reactions and solubility products are tabulated in (Table 2). Water column dissolved inorganic carbon (DIC) concentrations were calculated based on charge balance using the concentration of all major ions in solution (Crowe et al., 2008). Activity coefficients (γ) for the major ions in solution (γ) were calculated with the Debye-Hückel equation (6), which relates γ to z and I;

$$log\gamma_i = -0.5z_i^2\sqrt{I} \tag{6}$$

As γ is a function of the ionic strength of the lake waters (I), we calculated this using equation (7);

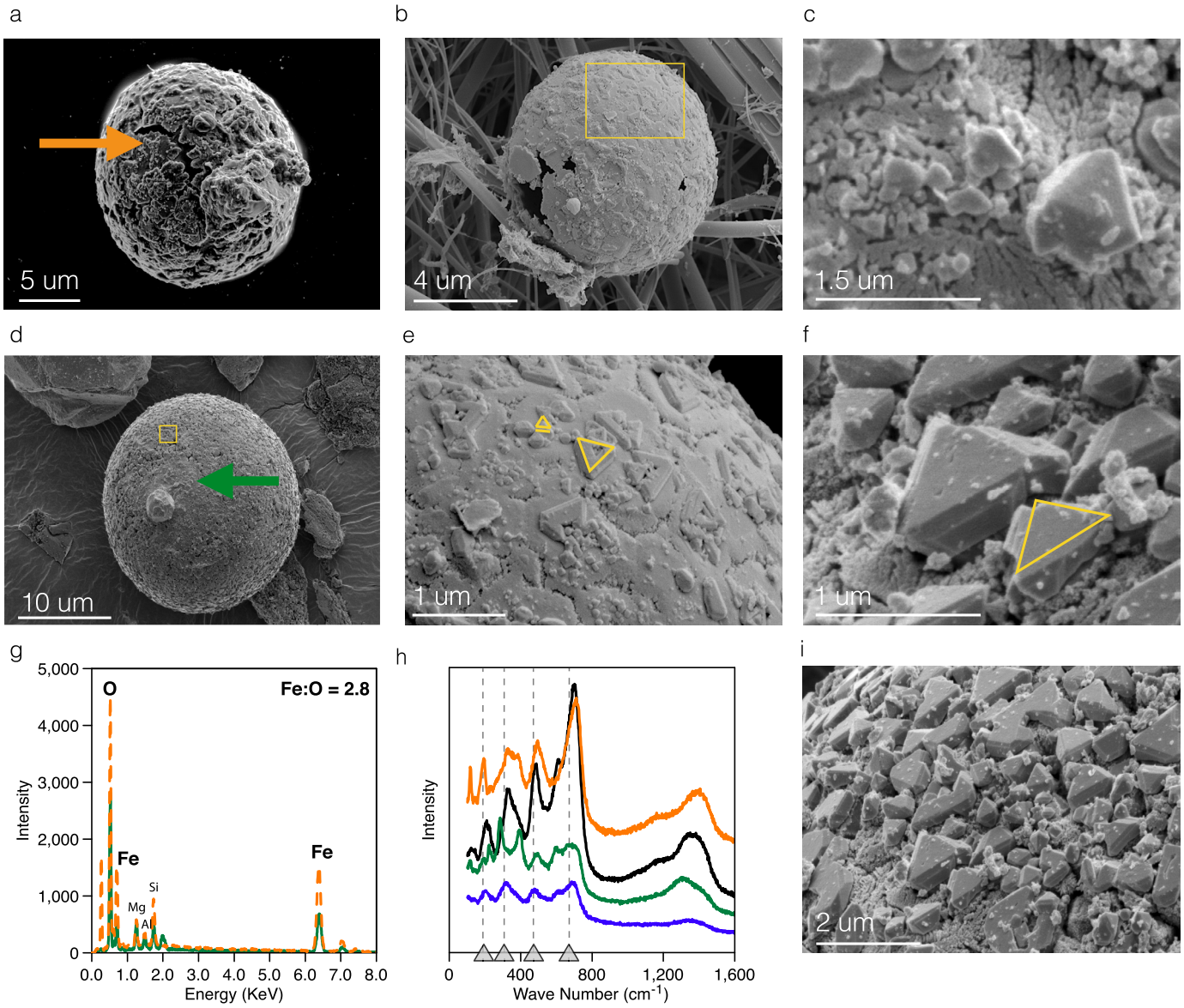

Fig. 4. Authigenic magnetite morphologies in the Malili lakes. **a)** Water column magnetite framboid captured in the LM deep sediment trap. Orange arrow indicates EDS spot location and corresponds to orange spectra in (g). **b)** Water column magnetite framboid captured in the LT deep sediment trap. **c)** A close up image of the framboid surface from (a). **d)** Magnetite framboid preserved in the LM sediment. Green arrow indicates EDS spot location and corresponds to green spectra in (g). **e)** A close up image of the framboid surface from (b), displaying immature magnetite octahedra. **f)** A close up image of the framboid surface from (d), displaying well-formed euhedral magnetite octahedra with identifiable crystal faces (111). **g)** SEM-EDS spectra of the framboids from (a) and (d). The orange and green arrows demarcate the EDS spot locations and corresponding spectral curves with the same colors from (a) and (d) respectively. Both framboids have Fe:O stoichiometry diagnostic of magnetite (see Fig. 6). **h)** Raman spectrum of sediment framboids from LM. Solid spectra correspond to 4 different framboids. Grey triangles on the x-axis correspond to prominent spectral bands for magnetite (Cornell and Schwertmann, 2003; Shebanova and Lazor, 2003). We observe diagnostic magnetite peaks at wave numbers ~306, ~450–490, ~538 and ~668 (cm^{-1}) (Shebanova and Lazor, 2003), with second order scattering between 1200–1400 cm^{-1}. **i)** A close up image of the framboid surface from (d), displaying nanoscale octahedral magnetite crystals.

Table 2
Mineral reactions used to calculate saturation indices in Fig. 1.

Mineral reaction	K_{sp}	Database
Magnetite $Fe_3O_4 + 8H^+ = 2Fe^{3+} + Fe^{2+} + 4H_2O$	2.53E+03	PHREEQC
Siderite $FeCO_3 = Fe^{2+} + CO_3^{2-}$	5.75E-11	PHREEQC
Goethite $FeOOH + 3H^+ = Fe^{3+} + 2H_2O$	3.10E+00	PHREEQC
Ferrihydrite $Fe(OH)_3 + 3H^+ = Fe^{3+} + 3H_2O$	1.55E+03	PHREEQC
Carbonate Green Rust $Fe_6(OH)12CO_3 + 13H^+ = 4Fe^{2+} + 2Fe^{3+} + HCO_3^- + 12H_2O$	1.26E+39	PHREEQC

$$I = \frac{1}{2}\sum m_i z_i^2 \quad (7)$$

where m_i and z_i are the molality and charge of each ion respectively. Water column dissolved Fe(III) concentrations in LM and LT were calculated assuming equilibrium ($SI = 0$) with either goethite or ferrihydrite as the solubility controlling phase.

2.6. Scanning electron microscopy (SEM)

Anoxically preserved water column and sediment samples were treated using a 1% osmium tetroxide solution buffered with 0.1 M PIPES at pH 6.8. Filters were rinsed gently with MQ water and then dried using an ethanol dehydration series. The filters were critical-point-dried using a Samdri795 (Toosimis Research Corporation). The filters were attached to a 12.5 mm stub and coated with 5 nm of iridium to ensure conductivity. The filters were imaged on a Helios FIB-SEM (FEI, Helios NanoLab 650) equipped with field emission gun. Fe(III) oxyhydroxides were confirmed through energy-dispersive X-ray spectroscopy (EDS) and elemental compositions determined based on X-ray fluorescence at the relevant emission energies for Fe, C and O.

2.7. Raman spectroscopy

Magnetically separated grains from LM sediment (section 2.2 above) were mounted in epoxy, and polished using a micro-diamond paste. Raman spectroscopy was conducted using a Horiba Ltd. XploRa Plus μ-Raman spectrometer using a green laser ($\lambda =$ 532 nm) and a 100× objective focused down to a spot ~1 μm in diameter, which provided a power at the sample surface of 2.5 mW. Spectral slit width was set at 100 μm and the confocal hole was kept at 300 μm. Data were collected during three cycles of 30 s to optimize the full width at half-maximum of resolved Raman bands, while minimizing possible effects of heating or oxidation.

3. Results

3.1. Fe-speciation

Canonically reactive Fe (Fe_{HR}; Table 1), which is thought to represent Fe-species reactive towards anaerobic microbial respiration and chemical reduction (Canfield et al., 1992), is the largest component (>90%) of the total Fe pool in suspended and deposited material from both LM and LT (Fig. 3, Table 3 and Table 4). Analyses of water column particles collected from sediment traps deployed above and below each lake's chemocline, as well as their bottom sediments, reveal Fe mineral transformations that take place both during transport through the water column and during early diagenesis in the uppermost deposited sediments. The speciation of Fe in sedimenting material from LM and LT is similar, and both shallow and deep sediment traps capture Fe that is mostly in the reactive, Fe_{HR}, form (Fig. 3 and Table 3). This Fe_{HR} is dominated by Fe_{Aca} (operationally defined as siderite), $Fe(III)_{HCl}$ (operationally defined as ferrihydrite) and Fe_{Dith} (operationally defined as goethite) extractable phases. Comparison between the shallow and deeps traps in LM, reveals these three pools together account for 83% and 70% of the total particulate Fe recovered in the shallow and deep traps, respectively, whereas in LT they account for 79% and 77%, respectively (Fig. 3, Table 3). Fe_{HR} dominates the total Fe pool (>90%) in both the shallow and deep traps in both lakes, and little variability in the abundance of Fe_{HR} is observed between these depths, implying inter-conversion of the different forms of Fe_{HR} directly within the water column. These pools also comprise Fe(III) mineral phases that are energetically favorable electron acceptors for anaerobic microbial respiration under standard-state conditions (Stumm and Morgan, 1988). The strong flux of Fe_{HR} thus provides an ample potential source of Fe(III), which through microbial respiration can be converted to, and accumulate as, Fe(II) under anoxic conditions.

Table 3
Water column Fe-speciation results.

Phase	Towuti (LT) 2015 110 m % of Fe_{Tot}	Towuti (LT) 2015 160 m % of Fe_{Tot}
Fe_{NR}	10	6
Fe_{HR}	90	94
$Fe_{(II)}$	14	18
$Fe_{(III)}$	77	77
Fe_{Aca}	7	5
$Fe(II)_{HCl}$	4	11
$Fe(III)_{HCl}$	39	32
Fe_{Dith}	33	41
$Fe_{Oxa(II)}$	2	2
$Fe_{Oxa(III)}$	5	4
$Fe_{Non\ Magnetic}$	94	74
$Fe_{Magnetic}$	6	25
$Fe_{Non\ Magnetic\ Oxalate\ Extractable}$	0.5	1
Total Fe (μg)	436	740
Phase	Matano (LM) 90 m % of Fe_{Tot}	Matano (LM) 130 m % of Fe_{Tot}
Fe_{NR}	7	6
Fe_{HR}	93	94
$Fe_{(II)}$	29	41
$Fe_{(III)}$	64	53
Fe_{Aca}	24	23
$Fe(II)_{HCl}$	1	15
$Fe(III)_{HCl}$	17	8
Fe_{Dith}	41	39
$Fe_{Oxa(II)}$	3	3
$Fe_{Oxa(III)}$	6	6
$Fe_{NonMagnetic}$	99	96
$Fe_{Magnetic}$	0	4
$Fe_{NonMagnetic\ Oxalate\ Extractable}$	1	1
Total Fe (μg)	525	948

The $Fe(III)_{HCl}$ pool, traditionally thought to represent the form most easily accessed for microbial respiration (Lovley and Phillips, 1986a), delivered to the lakes' anoxic waters is consumed directly within the water column and is thus quantitatively converted to dissolved Fe(II) and Fe(II)-bearing minerals (Table 3, Fig. 3). In LT, there is a minor increase in $Fe(III)_{HCl}$ between the shallow and deep traps, which is generated from the oxidation of Fe(II) at the chemocline, before it is consumed and converted to Fe(II) in the anoxic waters below the deep sediment trap (Table 4). In LM, reduction of the $Fe(III)_{HCl}$ pool begins between the two sediment traps (Table 4), and in both cases, dissolved Fe(II) accumulates within the water column of each lake. Equilibrium speciation calculations reveal that waters below the chemoclines in both LM and LT are supersaturated with respect to magnetite (Fig. 2d). Waters in LT are undersaturated with respect to siderite and carbonate green rust, while waters in LM are undersaturated with respect to green rust and moderately supersaturated with respect to siderite (Fig. 2d). Comparing the speciation of Fe captured in the upper sediment traps and Fe buried in the uppermost sediments reveals that reduction of the $Fe(III)_{HCl}$ pool takes place between these depths (Table 3, Table 4). In LT, consumption of the $Fe(III)_{HCl}$ pool occurs between the lower sediment trap and the sediment water interface, and $Fe(III)_{HCl}$ is absent from the underlying sediments. Due to this Fe(III) reduction the deep sediments of LM and LT receive negligible $Fe(III)_{HCl}$ (Table 4). Reduction of Fe(III) in the water column is also commensurate with increases in the proportion of extractable Fe(II) bearing phases Fe_{Oxa} (magnetite) and Fe_{Aca}, which in the deep traps increases by over 42% in LM and 25% in LT,

Table 4
Fe fluxes in the Malili lakes.

Sediment trap samples	Magnetite flux (mmol m^{-2} yr^{-1})	Fe_{Aca} flux (mmol m^{-2} yr^{-1})	$Fe(III)_{HCl}$ (mmol m^{-2} yr^{-1})	$Fe(III)_{Dith}$ (mmol m^{-2} yr^{-1})	Total $Fe_{HR}(II)$ flux (mmol m^{-2} yr^{-1})	Total $Fe_{HR}(III)$ flux (mmol m^{-2} yr^{-1})	Magnetite production (mmol m^{-2} yr^{-1})	Fe(III) reduction (mmol m^{-2} yr^{-1})
Matano, 90 m	11	28	19	46	32	73	8	52
Matano, 130 m	19	47	16	78	84	107		
Towuti, 110 m	13	13	73	63	26	145	7	30
Towuti, 160 m	20	15	101	129	56	245		
Sediment samples								
Matano Core Top (0.25 cm)	ND	ND	ND	ND	ND	ND	ND	ND
Matano Core Bottom (20 cm)	ND	ND	ND	ND	ND	ND		
Towuti Core Top (0.25 cm)	29	52	0	134	84	153	0	31
Towuti Core Bottom (40 cm)	27	57	0	111	114	129		

relative to the upper sediment traps (Fig. 3, Table 4). By contrast, the flux of Fe_{Dith} increases by 41% and 52% between the upper and lower traps in LM and LT, respectively (Table 4). In LT, however, Fe_{Dith} fluxes captured by the lower sediment trap are similar to those recorded in the bottom sediments (Fig. 3, Table 4), revealing that Fe_{Dith} is not reduced in the water column or deep sediments, and is relatively stable under ferruginous conditions in the Malili lakes.

Comparisons of magnetite fluxes recorded in the water columns and sediments reveal that most authigenic magnetite in LM and LT forms in the water column, with little modification in the underlying sediments. Magnetite fluxes to the lower sediment traps are 42% and 35% greater than the upper sediment traps from LM and LT, respectively (Fig. 3f and Table 4). This demonstrates magnetite formation directly within the water column at depths between the two sediment traps. In LT, magnetite fluxes to the upper sediments are also greater than the lower sediment traps (Fig. 3f and Table 4), and this indicates further magnetite formation, likely in the deep waters and the very uppermost deposited sediments. Throughout the upper 45 cm of the LT sediments, however, the flux of magnetite is roughly constant (Fig. 3f) revealing a lack of net magnetite formation or dissolution. This demonstrates that, while magnetite contains Fe(III), this Fe(III) is poorly biologically reactive and it is not further reduced in the sediment. Water column magnetite formation is thus the principal source of authigenic magnetite to the underlying sediments in LT, and once deposited is not subject to further Fe(III) reduction or other diagenetic modification.

3.2. Microscopy

We confirmed the presence of magnetite in the water columns and sediments of LM and LT using electron microscopic techniques and these analyses revealed different forms of magnetite that can be attributed to both authigenic and detrital origins. In the deep sediment traps, for example, we observed magnetite framboids (Fig. 4), which are clearly authigenic (Fig. 4 and Fig. 5a-f), as well as irregularly shaped partly weathered grains of likely detrital provenance (Fig. 5g-i). Many of the framboids appear to be hollow and detailed observations of framboid surfaces reveal that they are comprised of aggregates of nano-scale euhedral, octahedral crystals – a common crystal habit of magnetite (Fig. 4c, e, f). Micro-chemical analyses confirmed that these crystal aggregates had the 3:4 Fe:O stoichiometry diagnostic of magnetite (Fig. 4g, h and Fig. 6). Raman microspectroscopy yielded well-resolved reflections at wavenumbers (~310, ~450-490 and ~700 cm^{-1}), which correspond to the primary E_g, T_{2G} and A_{1G} vibrational modes that are diagnostic of magnetite (Shebanova and Lazor, 2003) (Fig. 4h). SEM-EDS analyses reveal that at the 95% confidence interval, the composition of framboids from the Malili lakes and the magnetite mineral standard are statistically indistinguishable (p value = 0.786) (Fig. 6).

4. Discussion

4.1. Magnetite formation, Fe(III) reduction, and Fe recycling

Magnetite formation in LM and LT is biologically induced, as it is associated with microbial reduction of the biologically reactive Fe(III) in the water column and uppermost sediments. Magnetite formation thus represents an important sink for microbially produced Fe(II). Fluxes of magnetite below the chemoclines of LM and LT are commensurate with the conversion of $Fe(III)_{HR}$ to $Fe(II)_{HR}$, which indicates Fe(III) reduction within this depth interval. Between the upper and lower sediment traps, magnetite formation accounts for 16% and 24% of this Fe reduction, respectively (Table 4). In LT, there is continued conversion of $Fe(III)_{HR}$ to $Fe(II)_{HR}$ in the anoxic waters between the lower sediment trap and uppermost sediments and magnetite formation accounts for 31% of this (Table 4). Biologically induced pelagic magnetite formation therefore represents a substantial sink for Fe(II) resulting from the microbial reduction of $Fe(III)_{HR}$ species directly in the water columns of LM and LT.

The $Fe(III)_{HCl}$ delivered to the upper sediment trap of LT is entirely converted to magnetite and $Fe(II)_{Aca}$ in the water column and this implies that an appreciable fraction of the $Fe(III)_{HCl}$ delivered to the lake is preserved as magnetite in the sediments. We note that while the Fe_{Aca} fraction is canonically attributed to siderite, the deep waters of LT are modestly undersaturated with respect to siderite, implying that the Fe_{Aca} fraction might represent other highly reactive reduced Fe minerals, like poorly crystalline Fe(II)-bearing clays. The flux of $Fe(III)_{HCl}$ delivered to the upper sediment trap is 73 mmol m^2 yr^{-1}, and this compares with the sum of magnetite and $Fe(II)_{Aca}$ fluxes of 29 and 52 mmol m^2 yr^{-1} in the uppermost sediments, respectively (Table 4). The absence of $Fe(III)_{HCl}$ in these uppermost sediments demonstrates that it is quantitatively consumed in the water column and uppermost sediments, as noted above. Fe_{Dith} fluxes are similar in the lower sediment trap and uppermost sediment revealing a lack of consumption of the $Fe(III)_{Dith}$ pool and limited conversion of $Fe(III)_{HCl}$ to $Fe(III)_{Dith}$ under ferruginous conditions (Fig. 3, Table 4). Mass balance thus requires that the consumption of $Fe(III)_{HCl}$ in the water column is entirely tied to the production of magnetite (36%) and Fe_{Aca} (64%). Given that 66% of Fe within stoichiometric magnetite is also Fe(III), this indicates that 24% of the Fe(III) delivered to the upper sediment trap is ultimately preserved in magnetite, revealing that water column magnetite formation influences the export and burial of oxidized equivalents (Fe(III), reaction 3) and thus exerts a primary control on the redox budget of the underlying ferruginous sediments in both lakes.

The accumulation of dissolved Fe(II) in the water columns of LM and LT implies Fe recycling with potential to support Fe dependent microbial metabolisms. To constrain rates of conversion of the $Fe(III)_{HCl}$ pool to Fe(II) and rates of recycling, we compared

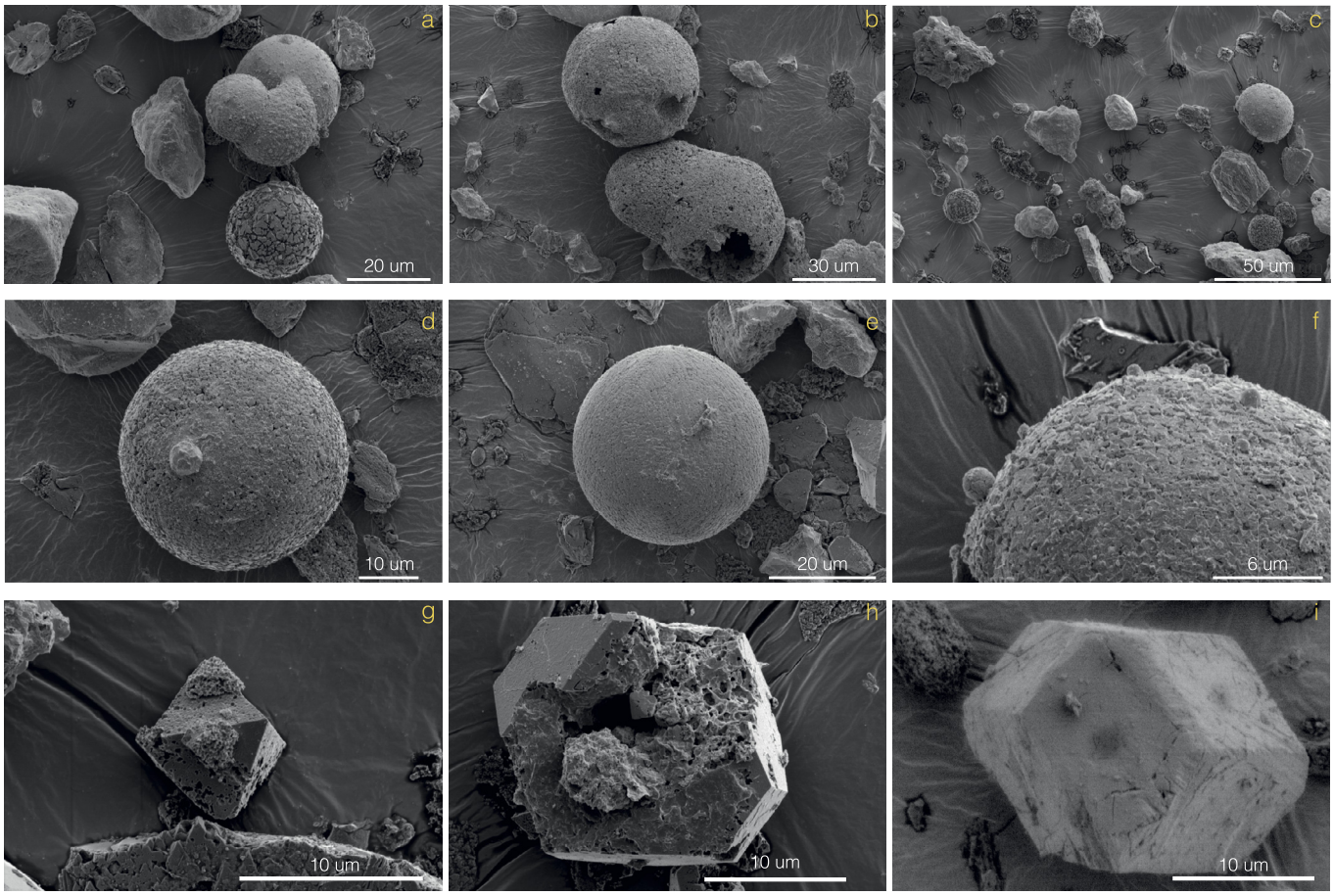

Fig. 5. Framboidal and detrital magnetite morphologies in the LM and LT sediment. Framboidal forms of magnetite in panels (**a-f**). We note that many of the framboids appear to be hollow. Detrital magnetite morphologies in panels (**g-i**). **g**) Octahedral crystal with pervasive dissolution pits. **h**) Cracked and broken euhedral crystal with pervasive surface dissolution pits. **i**) Rounded euhedral octahedral crystal (dodecahedral face (211)).

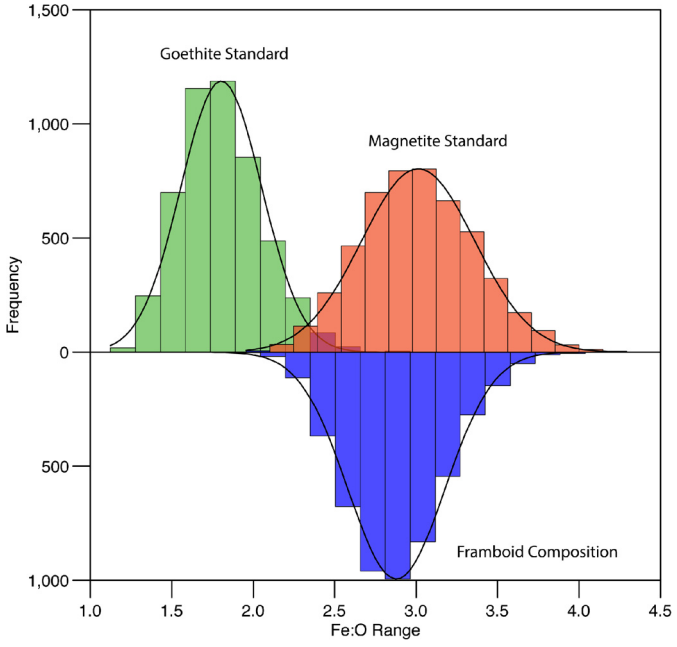

Fig. 6. SEM-EDS statistical results. To verify that the micro-chemical analyses of the SEM-EDS accurately differentiate magnetite from other Fe-oxide phases, we analyzed two pure Fe-mineral standards; magnetite (Fe_3O_4) and goethite (FeO(OH)). Plotted are histograms of the bootstrap resampled mean values of Fe:O compositions ($n = 10$), for the pure mineral standards compared to the combined water column and sediment magnetite framboid ($n = 17$) composition.

diffusive Fe(II) fluxes to the fluxes of $Fe(III)_{HCl}$ delivered to the upper sediment traps. In LT the diffusional flux of Fe(II) is 130 mmol m^2 yr^{-1} which, when divided by the delivery flux of $Fe(III)_{HCl}$ (73 mmol m^2 yr^{-1}) implies recycling of not more than 2 times. In LM the diffusional flux of Fe(II) is 55 mmol m^2 yr^{-1} which, when divided by the delivery flux of $Fe(III)_{HCl}$ (19 mmol m^2 yr^{-1}) implies recycling of not more than 3 times. Since $Fe(III)_{HCl}$ is the primary source of dissolved Fe(II), and much of this is converted to magnetite and Fe_{Aca}, the limited recycling implies that Fe dependent microbial metabolisms are ultimately restricted by both the delivery flux of $Fe(III)_{HCl}$ to the lake and its conversion to secondary Fe(II) bearing phases, which are ultimately removed through sedimentation and burial.

4.2. Implications for Precambrian environments

Our findings from LM and LT imply that pelagic magnetite formation can be an important mode of Fe delivery to ferruginous sediments and by extension suggest that magnetite derived from the Precambrian oceanic water column may have been a primary contributor to IF deposition. The source of Fe(III) (oxyhydr)oxide phases in the Precambrian oceans would have been direct photosynthetic Fe(II) oxidation (photoferrotrophy, reaction 4) (Thompson et al., 2019), or reaction of Fe(II) with oxygen produced through oxygenic photosynthesis in weakly oxygenated ocean surface environments (Cloud, 1973) (Fig. 1). Fe(II) would have been supplied through a combination of hydrothermalism and microbial Fe(III) reduction, which by analogy to modern ferruginous systems would likely have been tightly coupled to photosynthetic Fe(II) oxidation

(Llirós et al., 2015). Biologically induced magnetite formation in lakes LM and LT is linked to water column reduction of biologically reactive $Fe(III)_{HCl}$ supplied both from the catchment soils and through authigenic Fe cycling, as the likely source of Fe(II) in magnetite. Although the ultimate source of the primary Fe(III)-(oxyhydr)oxides in Precambrian oceans was likely different than in LM and LT, similar processes could be envisioned for magnetite formation. IF magnetite textures are clearly the result of secondary recrystallization and this obscures identification of primary mineral phases (Klein, 2005). Elemental compositions (Sun and Li, 2017), however, strongly imply a primary seawater source for the relevant precursor phases. Furthermore, lateral continuity in IF magnetite layers implies widespread deposition of precursor phases directly from the water column.

Formation of primary water column magnetite and its deposition in IFs would have been directly influenced by seawater chemistry. In LM and LT, magnetite forms under high degrees of supersaturation, at circumneutral pH, at <1 to 10s of μM Fe(II), and at mM concentrations of dissolved inorganic carbon (DIC) (Fig. 2). Notably, these Fe(II) concentrations are far lower than those thought to be required to induce magnetite formation in laboratory experiments (Lovley, 1991). Conditions similar to LM and LT, however, could be expected to support primary magnetite formation in the Precambrian oceans and, indeed, such conditions are in line with current reconstructions of Archean and Proterozoic seawater chemistry (Halevy et al., 2017; Thompson et al., 2019). Our observation of primary water column magnetite formation in LM and LT, even at modest Fe(II) and relatively high DIC concentrations suggests that the flux of iron-bearing particles to the Precambrian seafloor likely contained an appreciable fraction of magnetite. In LM and LT, such conditions also support the formation and deposition of an appreciable, though poorly defined Fe_{Aca} (canonically considered siderite) phase. Siderite precipitation in modern anoxic environments and laboratory experiments typically requires high degrees of supersaturation (Jimenez-Lopez and Romanek, 2004). Previous modeling of the Precambrian Fe cycle, however, suggests siderite may comprise an important fraction (up to 60%) of the sedimentary Fe sink, even under near equilibrium conditions ($SI_{Siderite}$ ~1) (Halevy et al., 2017), similar to LM and LT. In addition to magnetite, therefore, other possible primary phases like siderite (Halevy et al., 2017), green rust (Halevy et al., 2017; Zegeye et al., 2012) and greenalite (Tosca et al., 2016), may have been important contributors to IFs.

Recognition of magnetite formation in the water columns of LM and LT informs models of the Precambrian Earth system. During the Precambrian Eons, stronger greenhouse effects from high partial pressures of atmospheric CO_2 and CH_4 were likely required to sustain a clement climate on Earth, when the sun's luminosity was weaker (Reinhard and Planavsky, 2011; Rosing et al., 2010). These greenhouse gases would have regulated environmental conditions and would have also influenced the stability and thus deposition and preservation of different Fe-mineral phases. The mineralogy of IFs and the stability of the relevant minerals, therefore, can be used to constrain the concentrations of different greenhouse gases (CO_2 and CH_4) and thus their role in climate regulation at the time of IF deposition (Reinhard and Planavsky, 2011; Rosing et al., 2010). Some reconstructions suggest that the presence of magnetite in IFs reflects ocean conditions close to equilibrium with respect to magnetite, implying pCO_2 concentrations not much greater than today (~400 ppmv) (Rosing et al., 2010). Such low pCO_2 preclude it from acting as the primary greenhouse gas to warm planetary temperatures during the Precambrian Eons (Rosing et al., 2010). This, notably, contrasts with diagenetic models, which allow for conditions far from equilibrium with the ocean-atmosphere system (Reinhard and Planavsky, 2011) and yield estimates for atmospheric CO_2 concentrations up to 100 times present atmospheric levels (~40,000 ppmv). Magnetite formation in LM and LT takes place in the water column and under pCO_2 of −2.5 to −1.9 (~3000 to 10,000 ppmv) and this magnetite remains diagenetically stable under such conditions. Our observations in LM and LT thus suggest that magnetite could have formed in Precambrian oceans in equilibrium with an atmosphere that contained pCO_2 much greater than today. Furthermore, the apparent stability of magnetite in LM and LT implies that it would have been preserved in IFs, irrespective of similarly high pCO_2. Combined with other greenhouse gases, a ~10,000 ppmv CO_2 atmosphere falls short of, but approaches, a composition that would support warming sufficient for a clement climate (Ozaki et al., 2018). We note, however, both that our observation of magnetite stability is on relatively short (~1000 yr) timescales, and that magnetite may form and remain stable under much higher pCO_2. These uncertainties should be worked out in follow-on research.

The export of magnetite from the water columns of LM and LT contributes to the burial of oxidized equivalents in the underlying sediments and by extension implicates a role for coupled C and Fe cycling in setting Earth's surface redox budgets and the protracted oxidation of Earth's surface throughout the Precambrian Eons. Water column magnetite formation sequesters Fe(III) in a poorly biologically reactive form (reaction 5) that is not subject to subsequent Fe(III) reduction (reaction 6). This channels organic C away from Fe(III) reduction and into pathways that ultimately fuel CH_4 and H_2 production via both biological and photochemical reactions (ex., reaction 7) (Kasting, 2013; Ozaki et al., 2018) (Fig. 1). In LT, 23% of the biologically reactive $Fe(III)_{HCl}$ pool is converted to magnetite in association with microbial Fe(III) reduction. With global fluxes of up to 40 Tmol yr^{-1} reactive Fe to the Precambrian oceans (Thompson et al., 2019), and a similar fraction of conversion to magnetite, which is consistent with typical IF magnetite contents (Klein, 2005), we estimate that based on the Fe:C:H_2 stoichiometry of 4:1:2 (reactions 5 and 7), organic C channeled into fermentation and methanogenesis could fuel hydrogen fluxes of 4.6 Tmol yr^{-1}. This is nearly equivalent to twice the modern oxidant production through organic carbon burial in marine sediments (Holland, 2002). Key parameters that influence relevant Fe mineral formation pathways like pH, DIC (linked to pCO_2 through the carbonate system), Fe(II) concentrations, and Fe(III) production and consumption rates, as well as likely rates of microbial metabolism, would thus influence H_2 production rates and ultimately planetary oxidation rates.

4.3. Primary magnetite biosignatures

In LM and LT, primary magnetites often form in conspicuous framboidal morphologies (Fig. 4 and Fig. 5), which can thus be used to identify such primary magnetites in the rock record. Framboids are one of magnetite's most enigmatic crystal forms and natural occurrences have been sporadically observed in ancient sedimentary rocks and meteorites (Itambi et al., 2010; Suk et al., 1990). Biologically induced precipitation of magnetite framboids also occurs in response to microbial Fe(III) mineral reduction in laboratory experiments (O'Loughlin et al., 2015). This is distinct from biologically controlled magnetite formation, for example, through magnetosome biosynthesis in magnetotactic bacteria (Blakemore, 1975). Magnetosome magnetite takes the form of well-developed chains of octahedra (Posfai et al., 2013) and/or aggregates (Li et al., 2013), unlike the framboids of magnetite observed in LM and LT (Fig. 4). Spherical morphologies are also characteristic of magnetite produced during modern coal combustion (Goldhaber et al., 2004), however, based on the sedimentation rates in LM and LT, framboidal magnetites recovered from the deeper sediment intervals are thousands of years old (e.g., Vuillemin et al. (2019b)), conclusively ruling out such an anthropogenic source. We did not observe

framboidal magnetites in material recovered from upper sediment traps, but they were ubiquitous in deposited sediments from both LM and LT (Fig. 4, Fig. 5). Their absence from the upper sediment traps implies that they form under anoxic conditions, as the likely result of microbial Fe(III) reduction (Fig. 5).

Although the mechanisms causing magnetite framboid formation remain largely unknown, pyrite of similar morphology is known to form at redox interfaces in stratified water columns (Wilkin and Barnes, 1997). Hematite (Fe_2O_3), framboids of similar size and morphology have been observed in multiple Precambrian IFs (Lougheed and Mancuso, 1973). Leading models of framboid formation rely on the ferrimagnetic properties of the precursor Fe-phases that control framboid aggregation (Wilkin and Barnes, 1997), and thus it is unlikely that the framboids observed in IFs were originally deposited as poorly-magnetic phases, such as hematite. These hematite framboids, instead, have been attributed to post depositional oxidation of precursor pyrite framboids with biogenic origins (Lougheed and Mancuso, 1973). The oxidation of pyrite to magnetite, however, is accompanied by a significant molar volume reduction of 60%, and thus the preservation of the framboid microstructure during oxidation is unlikely (Wilkin and Barnes, 1997). At the same time, appreciable pyrite formation is not expected in the Archean oceans due to extremely low seawater sulfate concentrations (Crowe et al., 2014b), and consistent with the scarcity of sulfur in the Malili lakes system, we did not detect sulfur in any of our EDS analyses ruling out diagenetic pyrite oxidation (e.g., Suk et al. (1990)), as a likely mechanism for magnetite framboid formation in LM and LT. We alternatively suggest that the spheroidal hematite grains found in IFs were originally deposited as magnetite, and oxidized to hematite during subsequent diagenesis and or metamorphism. Such a provenance is supported by our observations from LM and LT. We also note that recrystallization of nano-magnetites to larger magnetite grains leads to textures commonly observed in IFs and in laboratory experiments even under low-grade pressure and temperature regimes (Li et al., 2013). There is thus ample evidence in support of the idea that magnetites in IFs represent the likely post depositional alteration products of primary nanoscale magnetite precipitates produced in response to pelagic microbial Fe respiration.

Beyond their likely contribution to terrestrial IFs, framboidal magnetites have also been observed in other rock types and meteorites, raising questions as to the role of biology in their formation (Bethke and Marshak, 1990; Suk et al., 1990). Our finding that magnetite framboids form in LM and LT in association with microbial Fe(III) reduction and are preserved in their sediments, combined with observations of biologically induced magnetite framboid formation in lab experiments (O'Loughlin et al., 2015), supports the idea that magnetite framboids may provide a relatively stable biomarker for microbial Fe respiration. Resolving the potential role for the use of framboidal magnetites in diagnosing Fe-biomineralization processes, however, requires both tighter constraints on the mechanisms of framboid formation, as well as more detailed geochemical and microbial fingerprinting of magnetite framboids themselves. The ability to visually identify framboids and, as we show here, determine their mineralogy through Raman microspectroscopy, holds considerable promise for detecting such potential biosignatures in sedimentary rocks from ancient ferruginous oceans on Earth, or remotely in extraterrestrial materials.

5. Conclusions

We find that in ferruginous Lakes Matano (LM) and Towuti (LT) in Indonesia, magnetite forms directly in the water column. This magnetite is one of the major products of microbial Fe(III) respiration and comprises an appreciable fraction of Fe exported to the underlying sediment, where it plays an important role in setting sediment redox budgets. These authigenic magnetites often take conspicuous framboidal forms, which given their links to microbial Fe(III) respiration may be diagnostic of this process and represent biosignatures. By analogy to LM and LT, we argue that similar processes in Precambrian ferruginous oceans would also have caused primary water column magnetite formation. We further argue that this water column magnetite formation would have contributed to the deposition of IFs, and like in LM and LT, magnetite deposition would have influenced the burial of oxidized equivalents in IFs and thus also the evolution of Earth's overall redox budget at this time. Observations that primary magnetite forms directly in ferruginous water columns has important implications for the interpretation of sedimentary mineralogical and isotopic features and for models of the Precambrian Earth system, including climate.

CRediT authorship contribution statement

SC conceived the research. KB, SC, RS, AF, AV, CM, SN, and JK participated in sample collection. KB and JB analyzed samples with input from AK, PK, MS and SC. KB, RF, and SC wrote the manuscript with input from all authors.

Declaration of competing interest

The authors declare that they have no known competing financial interests or personal relationships that could have appeared to influence the work reported in this paper.

Data and materials availability

The datasets and models generated during and/or analyzed during the current study are available from the corresponding author on reasonable request.

Acknowledgements

This work was funded through NSERC Discovery Grants to Sean A. Crowe (0487) and Roger Francois, the Canadian Foundation for Innovation, the Canada Research Chairs Program, and a UBC 4-Year Fellowship to Kohen Bauer, a GFZ Expedition grant to Jens Kallmeyer (F-0530), and SNSF grant to A. Vuillemin (P2GEP2 148621). Gethin Gowen assisted with the SEM imaging. Rhy McMillan helped with the preparation of samples for Raman microspectroscopy and Jan Axel Kitte aided in the fieldwork. This research was carried out with permission from the Ministry of Research, Technology, and Higher Education of the Republic of Indonesia (Ritekdikti, RISTEK), the Natural Resources Conservation Center (BKSDA), and the government of Luwu Timur of Sulawesi, Indonesia. The Director of Research Center for Limnology (RCL) - Indonesian Institute of Sciences (LIPI), Tri Widiyanto (RCL-LIPI), Aan Diyanto (RCL-LIPI) and staff of RCL-LIPI all contributed to the logistics of sampling in Indonesia.

References

Bethke, C.M., Marshak, S., 1990. Brine migrations across North America – the plate tectonics of groundwater. Annu. Rev. Earth Planet. Sci. 18, 287–315.
Blakemore, R., 1975. Magnetotactic bacteria. Science 190, 377–379.
Canfield, D.E., Raiswell, R., Bottrell, S., 1992. The reactivity of sedimentary iron minerals toward sulfide. Am. J. Sci. 292, 659–683.
Catling, D.C., Claire, M.W., 2005. How Earth's atmosphere evolved to an oxic state: a status report. Earth Planet. Sci. Lett. 237, 1–20.
Cloud, P., 1973. Paleoecological significance of the banded iron-formation. Econ. Geol. 68, 1135–1143.
Cornell, R.M., Schwertmann, U., 2003. The Iron Oxides: Structure, Properties, Reactions, Occurrences and Uses. John Wiley & Sons.

Crowe, S.A., Maresca, J.A., Jones, C., Sturm, A., Henny, C., Fowle, D.A., Cox, R.P., Delong, E.F., Canfield, D.E., 2014a. Deep-water anoxygenic photosynthesis in a ferruginous chemocline. Geobiology 12, 322–339.
Crowe, S.A., O'Neill, A.H., Katsev, S., Hehanussa, P., Haffner, G.D., Sundby, B., Mucci, A., Fowle, D.A., 2008. The biogeochemistry of tropical lakes: a case study from Lake Matano, Indonesia. Limnol. Oceanogr. 53, 319–331.
Crowe, S.A., Paris, G., Katsev, S., Jones, C., Kim, S.-T., Zerkle, A.L., Nomosatryo, S., Fowle, D.A., Adkins, J.F., Sessions, A.L., Farquhar, J., Canfield, D.E., 2014b. Sulfate was a trace constituent of Archean seawater. Science 346, 735–739.
Goldhaber, M., Callender, T., Reynolds, R., 2004. The geochemical and magnetic record of coal-combustion products in West Virginia reservoir sediments and soils. In: Geochemical Investigations in Earth and Space Science: A Tribute to Issac R. Kaplan, pp. 159–186.
Halevy, I., Alesker, M., Schuster, E.M., Popovitz-Biro, R., Feldman, Y., 2017. A key role for green rust in the Precambrian oceans and the genesis of iron formations. Nat. Geosci. 10, 135.
Holland, H.D., 2002. Volcanic gases, black smokers, and the Great Oxidation Event. Geochim. Cosmochim. Acta 66, 3811–3826.
Holland, H.D., 2006. The oxygenation of the atmosphere and oceans. Philos. Trans. R. Soc. Lond. B, Biol. Sci. 361, 903–915.
Itambi, A.C., von Dobeneck, T., Dekkers, M.J., Frederichs, T., 2010. Magnetic mineral inventory of equatorial Atlantic Ocean marine sediments off Senegal-glacial and interglacial contrast. Geophys. J. Int. 183, 163–177.
Jiao, Y.Y.Q., Kappler, A., Croal, L.R., Newman, D.K., 2005. Isolation and characterization of a genetically tractable photo autotrophic Fe(II)-oxidizing bacterium, Rhodopseudomonas palustris strain TIE-1. Appl. Environ. Microbiol. 71, 4487–4496.
Jimenez-Lopez, C., Romanek, C.S., 2004. Precipitation kinetics and carbon isotope partitioning of inorganic siderite at 25 degrees C and 1 atm. Geochim. Cosmochim. Acta 68, 557–571.
Johnson, C.M., Beard, B.L., Klein, C., Beukes, N.J., Roden, E.E., 2008. Iron isotopes constrain biologic and abiologic processes in banded iron formation genesis. Geochim. Cosmochim. Acta 72, 151–169.
Karlin, R., Lyle, M., Heath, G.R., 1987. Authigenic magnetite formation in suboxic marine sediments. Nature 326, 490–493.
Kasting, J.F., 2013. What caused the rise of atmospheric O-2? Chem. Geol. 362, 13–25.
Katsev, S., Crowe, S.A., Mucci, A., Sundby, B., Nomosatryo, S., Haffner, G.D., Fowle, D.A., 2010. Mixing and its effects on biogeochemistry in the persistently stratified, deep, tropical Lake Matano, Indonesia. Limnol. Oceanogr. 55, 763–776.
Klein, C., 2005. Some Precambrian banded iron-formations (BIFs) from around the world: their age, geologic setting, mineralogy, metamorphism, geochemistry, and origin. Am. Mineral. 90, 1473–1499.
Konhauser, K.O., Newman, D.K., Kappler, A., 2005. The potential significance of microbial Fe(III) reduction during deposition of Precambrian banded iron formations. Geobiology 3, 167–177.
Kostka, J.E., Nealson, K.H., 1995. Dissolution and reduction of magnetite by bacteria. Environ. Sci. Technol. 29, 2535–2540.
Lambrecht, N., Wittkop, C., Katsev, S., Fakhraee, M., Swanner, E.D., 2018. Geochemical characterization of two ferruginous meromictic lakes in the Upper Midwest, USA. J. Geophys. Res., Biogeosci. 123 (10), 3403–3422.
Li, Y.-L., Konhauser, K.O., Kappler, A., Hao, X.-L., 2013. Experimental low-grade alteration of biogenic magnetite indicates microbial involvement in generation of banded iron formations. Earth Planet. Sci. Lett. 361, 229–237.
Llirós, M., García-Armisen, T., Darchambeau, F., Morana, C., Triadó-Margarit, X., Inceoğlu, Ö., Borrego, C.M., Bouillon, S., Servais, P., Borges, A.V., 2015. Pelagic photoferrotrophy and iron cycling in a modern ferruginous basin. Sci. Rep. 5, 13803.
Lougheed, M., Mancuso, J., 1973. Hematite framboids in the Negaunee iron formation, Michigan; evidence for their biogenic origin. Econ. Geol. 68, 202–209.
Lovley, D.R., 1991. Magnetite formation during microbial dissimilatory iron reduction. In: Iron Biominerals, pp. 151–166.
Lovley, D.R., Phillips, E.J., 1986a. Availability of ferric iron for microbial reduction in bottom sediments of the freshwater tidal Potomac River. Appl. Environ. Microbiol. 52, 751–757.
Lovley, D.R., Phillips, E.J.P., 1986b. Organic matter mineralization with reduction of ferric iron in anaerobic sediments. Appl. Environ. Microbiol. 51, 683–689.
O'Loughlin, E.J., Gorski, C.A., Scherer, M.M., 2015. Effects of phosphate on secondary mineral formation during the bioreduction of akaganeite (β-FeOOH): green rust versus framboidal magnetite. Curr. Inorg. Chem. 5, 214–224.
Ozaki, K., Tajika, E., Hong, P.K., Nakagawa, Y., Reinhard, C.T., 2018. Effects of primitive photosynthesis on Earth's early climate system. Nat. Geosci. 11, 55–59.
Parkhurst, D.L., Appelo, C., 1999. User's guide to PHREEQC (version 2): a computer program for speciation, batch-reaction, one-dimensional transport, and inverse geochemical calculations. Water-Resour. Invest. 99, 312.
Posfai, M., Lefevre, C.T., Trubitsyn, D., Bazylinski, D.A., Frankel, R.B., 2013. Phylogenetic significance of composition and crystal morphology of magnetosome minerals. Front. Microbiol. 4.
Poulton, S.W., Canfield, D.E., 2005. Development of a sequential extraction procedure for iron: implications for iron partitioning in continentally derived particulates. Chem. Geol. 214, 209–221.
Reinhard, C.T., Planavsky, N.J., 2011. Mineralogical constraints on Precambrian p(CO2). Nature 474, E1–E2.
Rosing, M.T., Bird, D.K., Sleep, N.H., Bjerrum, C.J., 2010. No climate paradox under the faint early Sun. Nature 464, 744–U117.
Russell, J.M., Bijaksana, S., Vogel, H., Melles, M., Kallmeyer, J., Ariztegui, D., Crowe, S., Fajar, S., Hafidz, A., Haffner, D., Hasberg, A., Ivory, S., Kelly, C., King, J., Kirana, K., Morlock, M., Noren, A., O'Grady, R., Ordonez, L., Stevenson, J., von Rintelen, T., Vuillemin, A., Watkinson, I., Wattrus, N., Wicaksono, S., Wonik, T., Bauer, K., Deino, A., Friese, A., Henny, C., Imran, Marwoto R., Ngkoimani, L., Nomosatryo, S., Safiuddim, L., Simister, R., Tamuntuan, G., 2016. The Towuti Drilling Project: paleoenvironments, biological evolution, and geomicrobiology of a tropical Pacific lake. Sci. Drill. 21, 29–40.
Shebanova, O.N., Lazor, P., 2003. Raman spectroscopic study of magnetite (FeFe2O4): a new assignment for the vibrational spectrum. J. Solid State Chem. 174, 424–430.
Slotznick, S.P., Swanson-Hysell, N.L., Sperling, E.A., 2018. Oxygenated Mesoproterozoic lake revealed through magnetic mineralogy. Proc. Natl. Acad. Sci. USA 115, 12938–12943.
Stumm, W., Morgan, J.J., 1988. Aquatic chemistry; an introduction emphasizing chemical equilibria in natural waters. Current Contents/Agric. Biol. Environ. Sci., 18.
Suk, D., Peacor, D.R., Vandervoo, R., 1990. Replacement of pyrite framboids by magnetite in limestone and implications for palaeomagnetism. Nature 345, 611–613.
Sun, S., Li, Y.-L., 2017. Microstructures, crystallography and geochemistry of magnetite in 2500 to 2200 million-year-old banded iron formations from South Africa, western Australia and North China. Precambrian Res. 298, 292–305.
Thamdrup, B., Fossing, H., Jorgensen, B.B., 1994. Manganese, iron and sulfur cycling in a coastal marine sediment, Aarhus Bay, Denmark. Geochim. Cosmochim. Acta 58, 5115–5129.
Thompson, K.J., Kenward, P.A., Bauer, K.W., Warchola, T., Gauger, T., Martinez, R., Simister, R.L., Michiels, C.C., Llirós, M., Reinhard, C.T., Kappler, A., Konhauser, K.O., Crowe, S.A., 2019. Photoferrotrophy, deposition of banded iron formations, and methane production in Archean oceans. Sci. Adv. 5.
Tosca, N.J., Guggenheim, S., Pufahl, P.K., 2016. An authigenic origin for Precambrian greenalite: implications for iron formation and the chemistry of ancient seawater. Geol. Soc. Am. Bull. 128, 511–530.
Viollier, E., Inglett, P.W., Hunter, K., Roychoudhury, A.N., Van Cappellen, P., 2000. The ferrozine method revisited: Fe(II)/Fe(III) determination in natural waters. Appl. Geochem. 15, 785–790.
Vuillemin, A., Friese, A., Wirth, R., Schuessler, J.A., Schleicher, A.M., Kemnitz, H., Lücke, A., Bauer, K.W., Nomosatryo, S., Blanckenburg, F.v., 2019a. Vivianite formation in ferruginous sediments from Lake Towuti, Indonesia. Biogeosci. Discuss., 1–26.
Vuillemin, A., Wirth, R., Kemnitz, H., Schleicher, A.M., Friese, A., Bauer, K.W., Simister, R., Nomosatryo, S., Ordoñez, L., Ariztegui, D., 2019b. Formation of diagenetic siderite in modern ferruginous sediments. Geology 47, 540–544.
Walter, X.A., Picazo, A., Miracle, M.R., Vicente, E., Camacho, A., Aragno, M., Zopfi, J., 2014. Phototrophic Fe(II)-oxidation in the chemocline of a ferruginous meromictic lake. Front. Microbiol. 5, 9.
Wilkin, R.T., Barnes, H.L., 1997. Formation processes of framboidal pyrite. Geochim. Cosmochim. Acta 61, 323–339.
Zachara, J.M., Fredrickson, J.K., Li, S.-M., Kennedy, D.W., Smith, S.C., Gassman, P.L., 1998. Bacterial reduction of crystalline Fe (super 3+) oxides in single phase suspensions and subsurface materials. Am. Mineral. 83, 1426–1443.
Zegeye, A., Bonneville, S., Benning, L.G., Sturm, A., Fowle, D.A., Jones, C., Canfield, D.E., Ruby, C., MacLean, L.C., Nomosatryo, S., Crowe, S.A., Poulton, S.W., 2012. Green rust formation controls nutrient availability in a ferruginous water column. Geology 40, 599–602.
Zerkle, A.L., Claire, M., Domagal-Goldman, S.D., Farquhar, J., Poulton, S.W., 2012. A bistable organic-rich atmosphere on the Neoarchaean Earth. Nat. Geosci. 5, 359–363.